The Structure and Mesoscale Organization of Precipitating Stratocumulus

VERICA SAVIC-JOVCIC AND BJORN STEVENS

Department of Atmospheric and Oceanic Sciences, University of California, Los Angeles, Los Angeles, California

(Manuscript received 12 March 2007, in final form 6 August 2007)

ABSTRACT

Large-eddy simulations are used to explore the structure and mesoscale organization of precipitating stratocumulus. The simulations incorporate a simple, two-moment, bulk representation of microphysical processes, which by varying specified droplet concentrations allows for comparisons of simulations that do and do not develop precipitation. The boundary layer is represented over a large (25.6 km $\times$ 25.6 km) horizontal domain using a relatively fine mesh, thereby allowing for the development of mesoscale circulations while retaining an explicit representation of cloud radiative, dynamical and microphysical interactions on scales much smaller than the dominant eddy scale. Initial conditions are based on measurements made as part of the Second Dynamics and Chemistry of the Marine Stratocumulus field study (DYCOMS-II). The simulations show that precipitation is accompanied by sharp reductions in cloudiness and changes in flow topology. Mesoscale features emerge in all of the simulations but are amplified in the presence of drizzle. A cloud albedo of near 75% in the nonprecipitating simulation is reduced to less than 35% in the precipitating case. The circulation transitions from a well-mixed, stationary stratocumulus layer with closed-cellular cloud planforms to a stationary cumulus-coupled layer, with incipient open-cellular cloud planforms and sustained domain-averaged surface precipitation rates near 1 mm day^{-1}. The drizzling simulations embody many other features of observed precipitating stratocumulus, including elevated cloud tops in regions of precipitation and locally higher values of subcloud equivalent potential temperature. The latter is shown to result from the tendency for precipitating simulations to develop greater thermodynamic gradients in the subcloud layer as well as mesoscale circulations that locate regions of upward motion in the vicinity of precipitating cells.

1. Introduction

Drizzle is a diabatic process that affects the stratocumulus-topped boundary layer (STBL) and, thus, may play a role in setting the earth's radiative balance. Simple models suggest that drizzle alters the cloud albedo by affecting the cloud fraction (Albrecht 1989) and thickness (Pincus and Baker 1994). From a more dynamical point of view, drizzle provides a link between cloud microphysical processes and boundary layer circulations (Paluch and Lenschow 1991; Stevens et al. 1998).

The tendency of the STBL to precipitate—at times significantly—is by now well established (Brost et al. 1982a,b; Nicholls 1984). Recent field campaigns, the Second Dynamics and Chemistry of the Marine Stratocumulus field study (DYCOMS-II; Stevens et al. 2003) and the Eastern Pacific Investigation of Climate (EPIC; Bretherton et al. 2004), provide the clearest picture yet that drizzle is prevalent, long lasting, and locally intense (vanZanten et al. 2005; Comstock et al. 2005). These data further suggest that drizzle is associated with changes in PBL structure and cloud planforms. For instance, Paluch and Lenschow (1991) show that temperature and moisture are correlated on scales commensurate with the PBL depth, but anticorrelated on the mesoscale in the presence of drizzle; vanZanten et al. (2005) diagnose pools of elevated equivalent potential temperature, θ_e, within the subcloud layer of the regions associated with drizzle; Comstock et al. (2005) report higher horizontal variability in thermodynamic properties during drizzling events; while Stevens et al. (2005b) associate drizzle with open-cellular organization of clouds embedded into the otherwise closed-cellular stratocumulus, which they call pockets of open cells (POCs). Similarly, Sharon et al. (2006) suggest

Corresponding author address: Verica Savic-Jovcic, Department of Atmospheric and Oceanic Sciences, Box 951565, 7229 MSB, University of California, Los Angeles, Los Angeles, CA 90095-1565.
E-mail: verica@atmos.ucla.edu

DOI: 10.1175/2007JAS2456.1

that drizzle erodes stratocumulus decks and promotes patchy, broken clouds with cellular structure on the order of 10–20 km, which they call rifts.

From a theoretical perspective one would like to better understand the mechanisms and degree to which drizzle reorganizes the PBL circulations. Large-eddy simulations (LES) by Stevens et al. (1998) suggest that drizzle promotes cumulus-type circulations by increasing the buoyancy of downdrafts and therefore stabilizing the STBL, thus promoting decoupling and less deepening of the STBL. However, the small domain of their simulations raises questions about the reliability of their results—which essentially sample a single cumulus element in the decoupled regime. As they also note, the coarse vertical grid used in their study raises further questions about the fidelity of their simulations. Subsequent studies arrive at similar conclusions, although they debate the details of how precipitation interacts with and stabilizes the circulation (e.g., Ackerman et al. 2004). However, because the subsequent studies have also been for relatively small computational domains, they are too subject to the concerns that the statistics of the flow are insufficiently sampled to draw reliable conclusions and that the small domain inappropriately filters mesoscale circulations thought to be associated with drizzle.

In this study, we revisit the question of how drizzle affects the evolution of the STBL. Specifically, we ask: What is the structure of the drizzling STBL in terms of cloud and circulation organization? To what degree does LES capture the observed characteristics of the drizzling STBL? What is the extent of the agreement between the previous modeling work and ours? What generates the pools of elevated θ_e in the drizzling STBL? We address these questions by using a much larger, yet finer in the vertical, computational mesh than previous studies. The simulation domain of 25.6 km $\times$ 25.6 km $\times$ 1.5 km proves to be large enough to resolve numerous precipitating clouds that organize into loose networks reminiscent of open and closed cells, yet small enough to be computationally manageable. The initial conditions and forcing for the simulations are based on the second research flight (RF02) of DYCOMS-II (vanZanten and Stevens 2005) as summarized for the purposes of a case study by the Global Energy and Water Cycle Experiment (GEWEX) Cloud System Study (GCSS) boundary layer working group (A. S. Ackerman et al. 2008, unpublished manuscript).

This paper is organized as follows: section 2 describes our implementation of the University of California, Los Angeles (UCLA) LES along with the experiment setup. Section 3 discusses our simulations in light of available observations and previous theoretical/modeling work. In section 4 we explore the question why precipitating cells seem to be associated with pools of elevated θ_e. Issues pertaining to the scales sampled by the simulations, the effect of precipitation (and possibly other processes) thereon, and biases that may arise in simulations that do not represent mesoscale features are discussed in section 5. In section 6 we summarize our findings.

2. Methodology

This section describes the UCLA LES and our modifications to incorporate a bulk representation of warm rain microphysics. In addition, we describe the configuration of the simulations analyzed in this study.

a. Large-eddy simulation code

The base UCLA LES code is described by Stevens et al. (2005a). The radiative forcing is parameterized with a simple model of the net longwave radiative flux following Stevens et al. (2005a). Subfilter fluxes are modeled using the Smagorinsky–Lilly model. For scalars, however, the diffusivities are forced to decay exponentially with height, as having a nonzero near-surface eddy diffusivity allows for a smoother match to the surface boundary conditions. This forces all of the dissipation to be carried by the advection schemes at distances more than a few hundred meters above the surfaces. Stevens et al. (2005a) showed that, for the UCLA LES, this choice of representation of subfilter fluxes, while ad hoc, gives the most appropriate representation of entrainment and hence better simulations of stratocumulus compared to observations.

b. Microphysics

With a mind toward computational efficiency we introduce a simple model of microphysical processes that follows Seifert and Beheng (2001, 2006). Our interest is on the impact of precipitation on the surrounding flow, not on the details of its formation. We did experiment with other bulk representations of microphysical processes in stratocumulus (Khairoutdinov and Kogan 2000) with the main result being that lower droplet concentrations were required to produce the same rate of precipitation. Our interests also motivate a simplification to the Seifert and Beheng approach by maintaining the cloud water in equilibrium with a specified number concentration. Thus, only two additional prognostic equations must be solved—one for drizzle mass mixing

ratio, r_r, and another for number mixing ratio of drizzle, n_r—these being:

$$\frac{\partial r_r}{\partial t} = C_{cc}(r_c, r_r; m^*, n_c) + C_{cr}(r_c, r_r) + E(r_r, r_v, r_s, n_r) + \frac{\partial}{\partial x_3}\upsilon_r(r_r, n_r)r_r - \upsilon_i\frac{\partial r_r}{\partial x_i} + \frac{\partial}{\partial x_i}\left(K_h\frac{\partial r_r}{\partial x_i}\right), \quad (1)$$

$$\frac{\partial n_r}{\partial t} = \frac{1}{m^*}C_{cc}(r_c, r_r; m^*, n_c) + C_{rr}(r_r, n_r) + \frac{1}{m_r}E(r_r, r_v, r_s, n_r) + \frac{\partial}{\partial x_3}\upsilon_n(r_r, n_r)n_r - \upsilon_i\frac{\partial n_r}{\partial x_i} + \frac{\partial}{\partial x_i}\left(K_h\frac{\partial n_r}{\partial x_i}\right). \quad (2)$$

Here microphysical processes are represented in terms of intra- and interspecies interactions of the cloud droplets and drizzle drops, neglecting breakup. For instance, C_{cc} and C_{rr} represent intraspecies interactions of cloud droplets and drizzle drops (i.e., autoconversion and self-collection), respectively,[1] while C_{cr} denotes interspecies interactions of drizzle drops and cloud droplets (i.e., accretion); E symbolizes evaporation. For the sake of simplicity and because drizzle drops are small, our formulation excludes ventilation effects. Sedimentation utilizes mass- and number-weighted mean fall velocities, denoted respectively by υ_r and υ_n. In the above, r_c and n_c are mass and number mixing ratios for the cloud droplets, respectively; r_c is constrained by the equilibrium assumption (assuming uniformity of thermodynamic quantities within a grid cell) and n_c is specified. The parameter m_r is mean mass of drizzle drops; r_s is saturation mixing ratio, r_v is water vapor mixing ratio, υ_i is a resolved-scale velocity vector component in a tensor form, and K_h is eddy diffusivity. Detailed expressions for C_{cc}, C_{cr}, C_{rr}, E, υ_r, and υ_n, as well as specific parameter values used by the scheme, are presented in appendix A.

To fully account for effects of precipitation on the STBL (Ackerman et al. 2004) we allow cloud droplets to sediment following A. S. Ackerman et al. (2008, unpublished manuscript), and as discussed in appendix A. However, the geometric standard deviation of droplet sizes, which enter into the calculation of the sedimentation flux, is set at 1.2, rather than the GCSS value of 1.5 because the former agreed better with the measurements of vanZanten et al. (2005).

[1] The r_r dependence in C_{cc} parameterizes the effects of spectral ripening.

Being a diabatic process, drizzle affects the dynamics of the STBL through its impact on the thermodynamic fields, total-water mixing ratio, r_t, and liquid-water potential temperature, θ_l. If drizzle reaches the surface, it dries and warms the whole PBL. Likewise, locally, the drizzle flux divergence and the divergence of cloud-droplet sedimentation flux contribute to the change in θ_l and r_t, and thus introduce a source term in these equations as follows:

$$\frac{\partial \theta_l}{\partial t} = -\upsilon_i\frac{\partial \theta_l}{\partial x_i} + \frac{\partial}{\partial x_i}\left(K_h\frac{\partial \theta_l}{\partial x_i}\right) + \frac{\partial F_r}{\partial x_3} - \left(\frac{L\theta_l}{c_pT}\right)\frac{\partial F_p}{\partial x_3}, \quad (3)$$

$$\frac{\partial r_t}{\partial t} = -\upsilon_i\frac{\partial r_t}{\partial x_i} + \frac{\partial}{\partial x_i}\left(K_h\frac{\partial r_t}{\partial x_i}\right) + \frac{\partial F_p}{\partial x_3}. \quad (4)$$

Here F_r is radiation flux, $F_p = \upsilon_r(r_r, n_r)r_r + F_c(r_c, n_c)$ is precipitation flux that includes both drizzle and cloud droplet sedimentation F_c, L is the enthalpy of vaporization, c_p is the isobaric specific heat, and T is the absolute temperature.

c. Numerical experiments

Our analysis is centered around a comparison of three simulations: the nondrizzling simulation (hereafter NS), in which precipitation development is restricted by prescribing a large cloud droplet number concentration (200 cm^{-3}); the drizzling simulation (hereafter DS), where drizzle readily develops because the number concentration of cloud droplets is kept artificially low (25 cm^{-3}); and the drizzling without evaporation simulation (hereafter DWES), where evaporation of drizzle is inhibited [$E(r_r, r_v, r_s, n_r) = 0$].

The configuration of the UCLA LES for our cases follows that of the ninth GCSS LES comparison (A. S. Ackerman et al. 2008, unpublished manuscript) except for the extension to a much larger domain, thereby embodying more grid points (512) in each of the horizontal directions, and a different specifications of cloud droplet concentrations (the GCSS specification was for $N_c = 55$ cm^{-3}). To review, the horizontal mesh has a 50-m spacing, and the vertical mesh is stretched, starting at 5 m near the surface, dilating following a $\sin^2$ law in the interior of the STBL, contracting again near the inversion to maintain a uniform 5-m spacing in a 125-m zone around the mean inversion height, and then dilating again so that the mesh spacing at the model top is about 80 m. Each simulation is carried forward for 6 h which provides sufficient time for meso-γ scales (Orlan-

ski 1975) of circulations to become evident on the domain.[2]

The large-scale forcings and initial and boundary conditions also follow the configuration for the experiments in the ninth GCSS comparison (A. S. Ackerman et al. 2008, unpublished manuscript). The Coriolis parameter f is determined at 31.5°N, and the large-scale divergence is set to 3.75×10^{-6} s^{-1}. The initial vertical profile for momentum is linear with a surface value of 3 m s^{-1} for the zonal and 9 m s^{-1} for the meridional component, increasing with height at a rate of 4.3 m s^{-1} km^{-1} and 5.6 m s^{-1} km^{-1}, respectively. Initial profiles of θ_l and r_t are well mixed within the STBL with values of 288.3 K and 9.45 g kg^{-1}. At the inversion, there is a sharp jump to values of 295 K and 5 g kg^{-1}, and above the inversion is a slight increase of θ_l and decrease of r_t, according to $(z - z_i)^{1/3}$ and $3\{1\text{—}\exp[(z_i - z)/500]\}$ for θ_l and r_t, respectively, where z is height in meters and $z_i = 795$ m is the initial inversion height.

Boundary conditions include surface pressure set to 1017.8 hPa; sensible and latent heat fluxes prescribed to 16 and 93 W m^{-2}, respectively; and surface stress fixed at $u_* = 0.25$ m s^{-1} and distributed into upward momentum fluxes with the bulk formulas, where the wind components and the magnitude of the horizontal wind are defined locally. By specifying surface fluxes we attempt to mimic the case of a Lagrangian evolution of the layer as it advects over progressively warmer waters. Such a strategy is also in accord with the sampling strategy employed during DYCOMS-II. Tests in which the sea surface temperature was allowed to evolve in time in a way that maintained the same mean fluxes lead to no appreciable differences in the simulations. For computational expediency the upper 250 m of the domain consists of a sponge layer with a damping coefficient that increases linearly with height to a value of 10^{-2} s^{-1}. Lateral boundary conditions are periodic and the domain is subjected to a Galilean transform of 5 and −5.5 m s^{-1} in the x and y directions, respectively.

3. The simulations

a. Structure and evolution of the flow

The development of drizzle in stratocumulus leads to profound changes in both cloud amount and organization. Although our simulations are for nocturnal stratocumulus, thereby circumventing any possible interactions with solar radiative processes, we visualize these changes in terms of the cloud albedo A, which we calculate following the simple prescription (e.g., Zhang et al. 2005)

$$A = \frac{\tau}{6.8 + \tau}, \tag{5}$$

where $\tau = 0.19\mathcal{L}^{5/6}N_c^{1/3}$ is the optical depth, N_c is the cloud-droplet number concentration, and $\mathcal{L} = \int_0^\infty r_l\rho_0\, dz$ is the liquid water path. Snapshots of A at the end of each simulation are shown in Fig. 1. Each can be argued to provide a compelling, but markedly different, realization of the stratocumulus-topped boundary layer.

In the absence of drizzle (Fig. 1, NS), the cloud adopts a closed-cell planform (e.g., Comstock et al. 2005; Agee 1984), where the cell centers are characterized by high reflectivity and cell walls are loci of low reflectivity, and in places may even be cloud free. Overall, the albedo for NS is relatively uniform with a domain-averaged value near 75%. In contrast, the development of significant drizzle (surface rain rates in the DS and DWES average near 1 mm day^{-1}, roughly corresponding to 30 W m^{-2}) leads to a much less reflective and spatially more variable cloud layer (Fig. 1, DS). The domain-averaged albedo in DS falls to less than 35%, which is less than half its value in the absence of drizzle. About one-third of the reduction in the albedo can be attributed to the Twomey effect (reduced scattering in the presence of fewer drops); if the albedo in NS is recalculated with $N = 25$ cm^{-3} (commensurate with droplet concentrations in DS), it falls to just under 60%. Thus, the bulk of the changes in the albedo are due to changes in the amount and distribution of the cloud water.

Indeed, the DS is topologically distinct from the NS (Fig. 1). By this we mean that the shape of the probability distribution function of liquid water path (LWP), and hence albedo, differ qualitatively. This is evident both in the probability distribution function shown in Fig. 2 and in spatial distribution of albedo. In the former we note that, while the overall distribution in the DS has shifted to the left, the emergence of a long tail differentiates it from the other distributions. This is somewhat less evident in the albedo plots because the regions of highest LWP in the DS also have fewer drops than the NS. The shift of the distribution to the left in the DS and DWES reflects the emergence of cloud-free regions in the precipitating simulations. While all simulations evince aspects of what is referred to as a closed-cellular structure, the high LWP cell centers in the DS are beginning to organize in loose networks that hint at an emergent open-cellular (bright walls, dim centers) pattern. These types of changes are consistent with behavior hinted at by previous simulations in relatively small domains (e.g., Stevens et al. 1998) as well as ob-

[2] A 6-h simulation integrated on 128 processors of an IBM POWER5 machine at NCAR takes 18.5 h of wall-clock time.

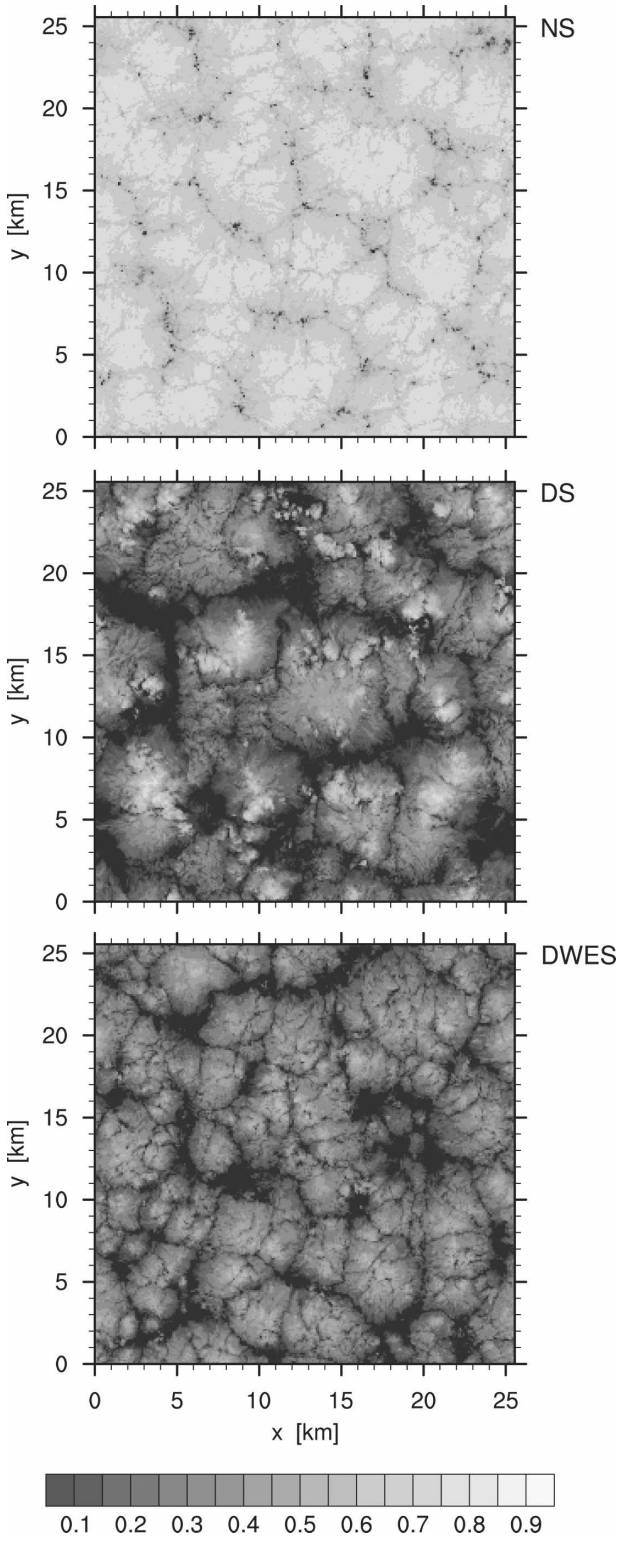

FIG. 1. Albedo, per Eq. (5), at the end of the sixth hour of simulations.

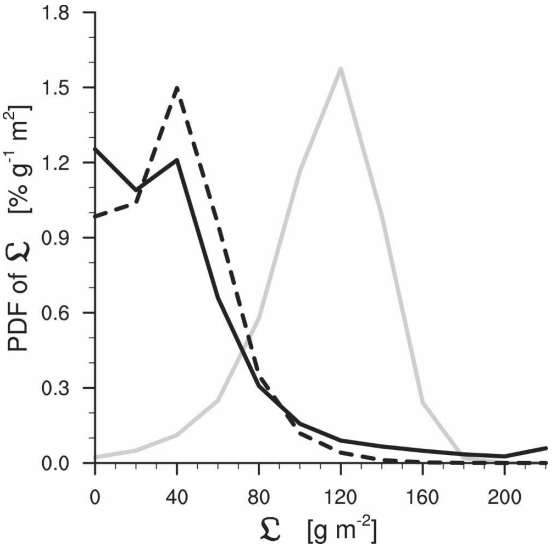

FIG. 2. Distribution of liquid water path in simulations: NS (solid gray line), DS (solid black line), and DWES (dashed black line).

servations contrasting precipitating versus nonprecipitating layers of stratocumulus (e.g., vanZanten et al. 2005; Comstock et al. 2005).

By preventing evaporation of precipitation-size drops in the DWES we both enhance the efficiency with which water is removed from the boundary layer and inhibit the tendency of drizzle to stabilize the subcloud layer with respect to the cloud layer. So doing leads to a simulation whose reflectivities are reduced to values only marginally larger than for the DS but which lack the underlying topological changes. Although the cloud field is more broken, there is little evidence of networks of high reflectivity, such as might be associated with underlying cumuliform convection. This suggests that, at least for this case, the evaporation of precipitation plays an important role in reorganizing the circulation and that, at least in the short term, this reorganization (embodied by compact regions of high reflectivity in the DS) has more to do with determining the overall albedo of the layer than does the tendency of drizzle to remove water from the cloud layer.

Our basis for associating drizzle with topological changes in the underlying flow is more readily evident in horizontal cross sections of θ_l', r_t', and w', both in the subcloud layer (Fig. 3) and in the cloud layer (Fig. 4). Here primes denote deviations from layer mean quantities. In the drizzling simulations (DS and DWES), these cross sections are overlaid with contours of spatially smoothed precipitation. Comparing the DS with the NS (Fig. 3) suggests that with the development of precipitation the open-cellular network of surface-

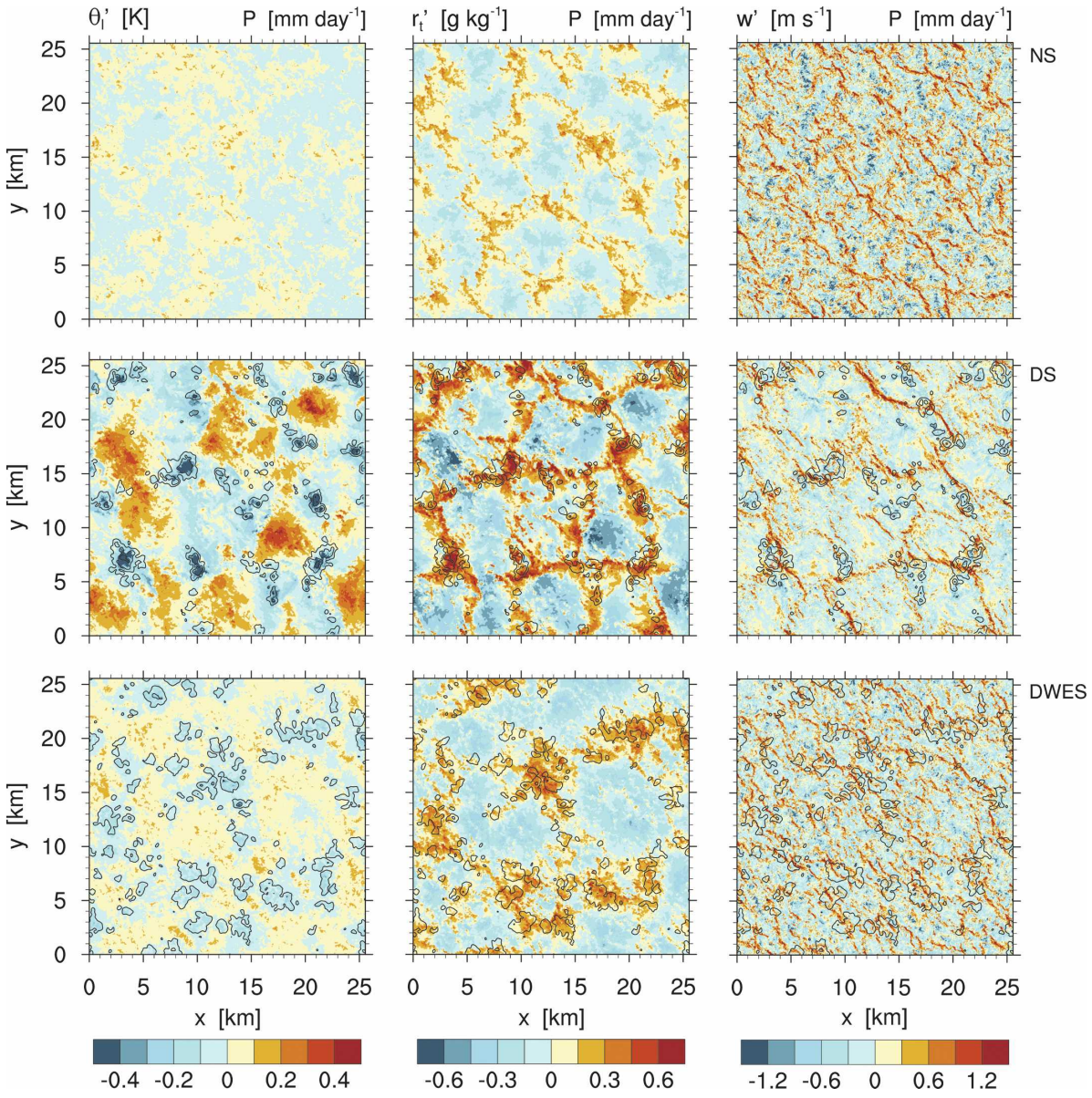

FIG. 3. Planar view of instantaneous perturbations from the horizontal mean values of θ_l, r_t, and w fields at 200-m level at the end of the sixth hour of three simulations. Precipitation contours that overlay the plots for DS and DWES are spatially smoothed for clarity, and have values of 2, 10, and 30 mm day^{-1}.

bound r_t anomalies both intensifies and becomes more positively skewed. Regions of positive anomalies appear to be loci of strong upward motion, precipitation, and cooler air (hence significantly lowered condensation levels). In the absence of drizzle the flow shows a more familiar picture of radiatively driven stratocumulus, wherein w' is more finely grained (Figs. 3 and 4), with upward and downward motions of more commensurate strength (note the paucity of strong downdrafts in the precipitating simulations). Although even in the NS the subcloud r_t' field evinces the underlying support for a more open-cellular structure, the imprint of such structure is less evident in the albedo.

A comparison of cross sections from the DS with those from the DWES (Figs. 3 and 4) suggests that the evaporation of drizzle is critical to these topological changes. In the absence of evaporation of precipitation-size drops, the open-cellular-like network is much less evident. Regions of precipitation, which are more regularly patterned, concentrated, and associated with strong fluctuations in the subcloud thermodynamic structure in the DS, are more widespread, less intense,

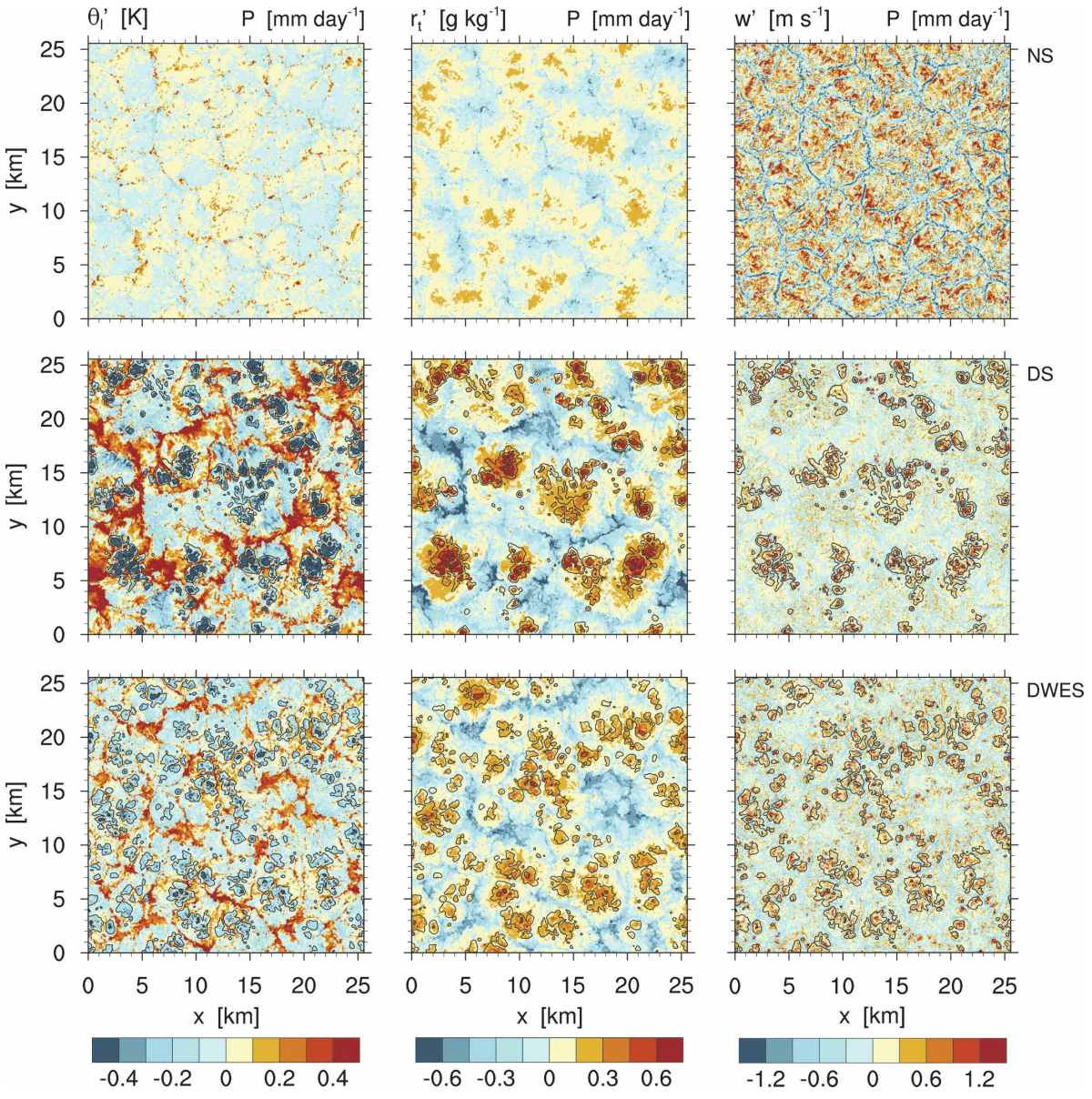

FIG. 4. As in Fig. 3 but for 700-m level.

and less apparently organized in the DWES. Although the subcloud moisture field (middle column in Fig. 3) shows mesoscale structure in both simulations, the low-level moisture maxima along which convection appears to organize are more diffuse in the DWES and more reminiscent of the patterns in the NS. As we shall see, this form of organization is more typical of well-mixed stratocumulus layers, with relatively little differentiation between cloud base in up- and downdraft regions of the flow. In the precipitating simulations, however, cloud base lowers in regions of precipitation and rises away from the precipitating regions, leading to a marked differentiation in cloud base. Such behavior is consistent with the visual record from the recent Drizzle and Open Cells in Marine Stratocumulus (DOCIMS) field study, which used the new National Center for Atmospheric Research/National Science Foundation (NCAR/NSF) Gulfstream V to target precipitating open cells as well as the photographic evidence from EPIC.

Many of the above discussed aspects of the simulations are also evident in Fig. 5, which shows vertical cross sections (or slices) of w' and the equivalent potential temperature, θ_e, in each of the three simulations, with cloud water and rain contours overlaid. Here the tendency of the DS to develop a circulation consisting

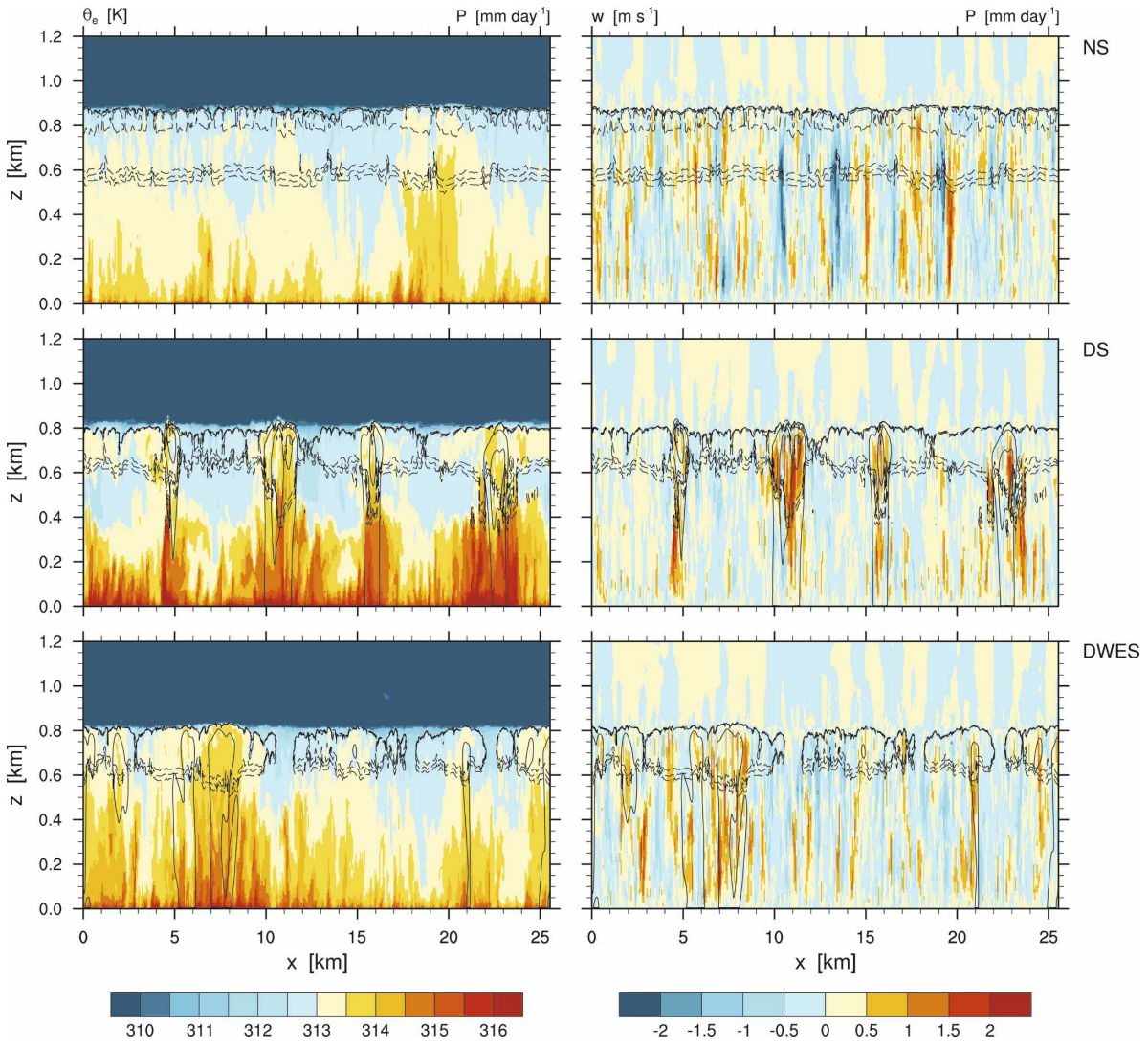

FIG. 5. Vertical cross sections of instantaneous θ_e and w fields at $y = 45$ m at the end of the sixth hour of simulations, overlaid with dashed contours of r_c with values of 0.01, 0.05, 0.1, and 0.5 g kg^{-1}. Plots for DS and DWES are additionally overlaid with solid contours of precipitation with values of 2, 10, and 30 mm day^{-1}.

of cumulus under stratocumulus is especially evident, with the precipitation strongly localized in the vicinity of updrafts rich in θ_e and a locally lower cloud base, that is, cumulus clouds. These cumulus clouds are noticeably associated with locally elevated cloud tops, a conspicuous feature of observations of precipitating boundary layers (cf. Paluch and Lenschow 1991; Vali et al. 1998; Stevens et al. 2005b; Petters et al. 2006) that was not well reproduced in the relatively coarse vertical resolution simulations of Stevens et al. (1998). These vertical cross sections highlight the important role downdrafts play in the NS, as compared to updrafts that are more dominant in the circulation of the DS.

Some of the changes associated with precipitation can be efficiently summarized by mean vertical profiles of selected quantities. Figure 6 shows how precipitation leads to a substantially shallower boundary layer and a significant reduction in liquid water and cloud fraction. Peak values of layer-averaged liquid water are reduced by more than half. The development of a tail in the cloud fraction extending down to 400 m and more pronounced gradients in thermodynamic quantities near this level, especially moisture (Siebesma et al. 2003), is often taken as a signature of more cumulus-coupled circulations. Because to a first approximation $\theta_e \approx \theta_l + (L/c_p)r_t$, the effects of the negative moisture gradients overwhelm the slight positive θ_l gradients so that the θ_e profiles follow more closely those of r_t, consistent with the cross sections in Fig. 5. The degree of differentiation between the cloud and subcloud layer thermody-

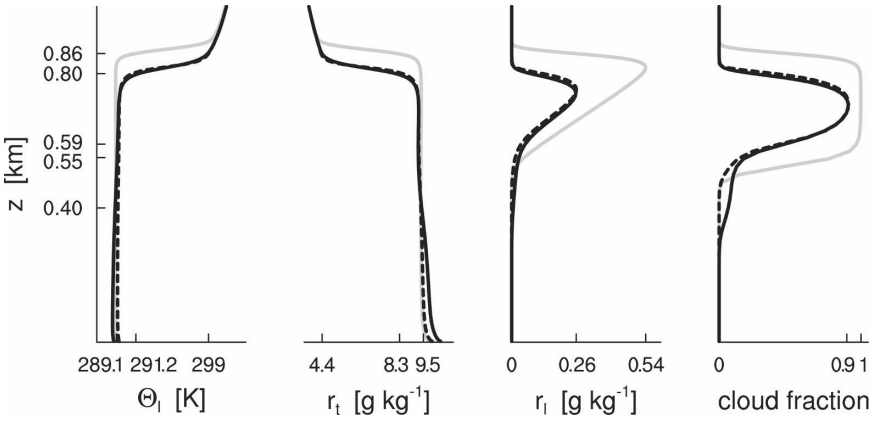

FIG. 6. Mean profiles of θ_l, r_t, r_l, and cloud fraction (panels from left to right, respectively), averaged over the last two hours of the simulation. Lines as in Fig. 2. Top four values on y axis represent the corresponding 2-h average of time series of cloud-top and cloud-base heights for NS and DS. Bottom value on y axis represents the lowest height where the profile of r_l is greater than 0.01 g kg^{-1}. Values on the x axes are BL averages, base- and top-of-transition-layer values of θ_l and r_t for DS, and maximum of r_l and cloud fraction within the boundary layer for NS and DS.

namic quantities are, however, not nearly as large as in the simulations by Stevens et al. (1998). Whether or not they are in conflict with the observations of vanZanten et al. (2005), who do not find significant vertical differentiation between the cloud and subcloud layers thermodynamic properties, is more difficult to ascertain because of the sampling strategy employed in their observational strategy. These features are absent from the DWES.

The tendency of precipitation to suppress the growth of the boundary layer is consistent with the weaker circulations. Figure 7 shows that the peak values of $\overline{w'w'}$ are reduced by nearly a factor of 3 and have a more bimodal structure (with a local minimum near cloud base) in the presence of drizzle. Such a profile of the vertical velocity variance is often associated with decoupling (Stevens 2000), although only in the case when precipitation is allowed to evaporate in the subcloud layer is such decoupling associated with the statistical trace of cumulus clouds. The third moment of w' is positive throughout the layer in both DS and DWES, indicative of a more surface-forced circulation irrespective of whether or not precipitation is allowed to evaporate. However, the locally increased value of $\overline{w'w'w'}$ in

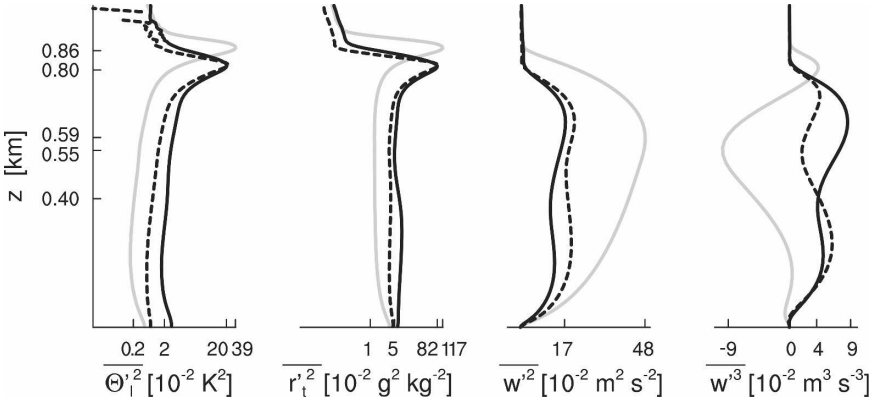

FIG. 7. Mean profiles of variances of θ_l and r_t with logarithmic horizontal axis, and variance and third moment of w (panels from left to right, respectively), averaged over the last two hours of the simulation. Choice of lines and values on y axis are as in Fig. 6. Values on x axes are as follows: minimum of variance in the boundary layer and maximum of variance at the interface layer for NS and DS for θ_l and r_t; maximum of w variance in NS and DS and maximum of $\overline{w'w'w'}$ in NS and DS, and minimum of $\overline{w'w'w'}$ in NS. The exception is the 0.08 value on the plot of $\overline{r_t'r_t'}$, which is a maximum of variance in the boundary layer of DS.

the cloud layer is also consistent with more cumulus-like circulations in the DS.

Variances in thermodynamic quantities are also shown in Fig. 7, but on a logarithmic scale. While the general trend toward more scalar variance to accompany reductions in $\overline{w'w'}$ is apparent, and larger mean-field gradients, the logarithmic scale deemphasizes the degree to which the DS exhibits greater scalar variance, even though values of $\overline{w'w'}$ in the DS are commensurate with those in the DWES. This is yet another indicator of topological changes in the flow that emerge only when precipitation is allowed to evaporate.

Much of the reduction in the intensity of the circulations in the presence of drizzle can be associated with reduced buoyancy fluxes, stemming in part from less radiative driving. These changes are evident in the profiles of the radiative, precipitation, and buoyancy fluxes in Fig. 8, where we note that the precipitation flux associated with NS is purely from the sedimentation of cloud droplets. Because the longwave radiative flux saturates for relatively small liquid water paths, the change in the radiative forcing among the simulations is not especially strong. So it is not surprising that nonprecipitating simulations with the radiative forcing reduced to match that of the DS (not shown) show this effect to be insufficient to explain the differences among the simulations. Indeed, the radiative flux divergence as a whole is less than the precipitation flux divergence at cloud top, let alone the differences in the radiative flux divergences between the precipitating and nonprecipitating simulations. For the most part, however, the effect of the precipitation flux does not project immediately onto the buoyancy field. Instead, this forcing is manifest in raising the condensation level of the cloud-top air, which acts to stabilize downdrafts through the mechanism discussed by Stevens et al. (1998). Indeed, strong downdrafts, whether they be driven by radiation or evaporation, are not particularly evident in either the DS or the DWES at either 200 or 700 m (see, e.g., Figs. 3 and 4).

The evaporation of precipitation in the DS (Fig. 8) is significant, but relatively less than reported by vanZanten et al. (2005). In DS about 37% of the precipitation makes it to the surface compared to just under 30% in the measurements. The evaporation of precipitation that we do see acts to stabilize the cloud layer with respect to the subcloud layer, and subcloud buoyancy fluxes are reduced. However because the evaporation of precipitation lowers the condensation level of subsequent updrafts, the buoyancy flux in the cloud layer increases. Although in our simulations these differences appear crucial, the transition to a decoupled flow can be sharp (e.g., Stevens 2000); hence it remains unclear to what extent the evaporation effect of drizzle is generally important, or just gives the simulations the extra kick necessary for them to decouple in this particular instance.

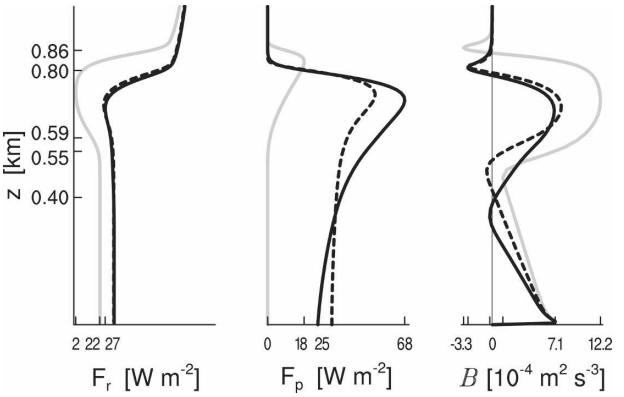

FIG. 8. Mean profiles of (left) radiation, (middle) downward precipitation, and (right) buoyancy flux averaged over the last two hours of the simulation. Choice of lines and values on y axis are as in Fig. 6. Values on x axes are as follows: for radiation flux, minimum and surface values for NS, and minimum for DS (left); for precipitation flux, maximum and surface values in NS and DS; and for buoyancy flux, maximum for NS and DS (right), zero reference line, and cloud-top minimum for NS.

Finally, we note, with the aid of Fig. 9, that the changes in the flow, documented above, are not simply transient features but persist over time scales that are large compared to a typical eddy turnover time of 10–20 min. Subsequent to the spinup of the simulations, global features such as the net surface precipitation, the cloud liquid water path, and the growth rate of the layer and of the domain-averaged turbulence kinetic energy (TKE) are remarkably constant. Clearly precipitation, while depleting the cloud layer of liquid water, does not lead to a collapse or more rapid demise of the cloud layer. The ability of the circulations to sustain a long-lived, persistently precipitating layer is consistent with observations by vanZanten et al. (2005) and Comstock et al. (2005), although it had been called into question by some earlier studies, and a somewhat lazy terminology that too often associates precipitation duration with cloud lifetimes. The time series of PBL depth (third panel in Fig. 9) also shows that the tendency of the precipitating layers to deepen less rapidly, as was evident in earlier work of Stevens et al. (1998), represents a systematic influence of weaker entrainment rates rather than a sudden adjustment to the development of precipitation. Interestingly, there is a slight tendency of the DS to deepen less rapidly than the DWES, despite slightly increased values of TKE. We speculate that this is due to a greater fraction of the TKE being carried by the variances in the horizontal wind in the DS, as the

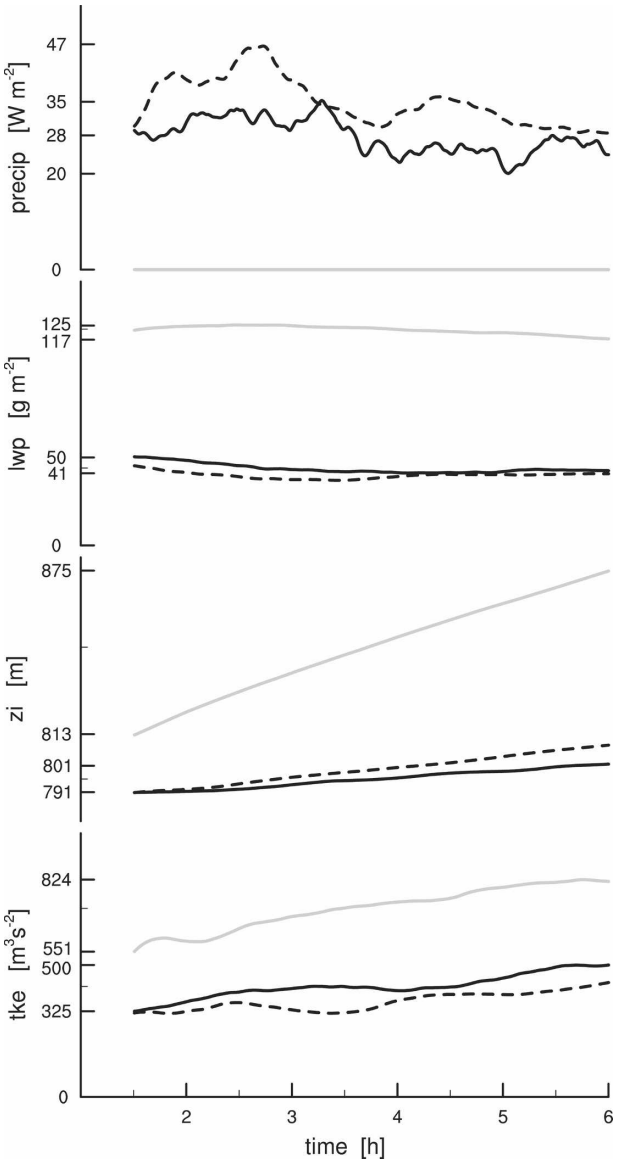

FIG. 9. Time series of domain-averaged surface precipitation, LWP, inversion height, and vertically integrated turbulence kinetic energy (panels from top to bottom, respectively). Line description as in Fig. 2. Values on y axes are as follows: minimum and maximum of time series of precipitation in all three simulations (top panel) and minimum and maximum of corresponding time series for NS and DS (lower three panels). Unlabeled tick marks on lower three panels represent mean values of the corresponding time series for NS and DS.

values of $\overline{w'w'}$ are smaller in the DS than in the DWES, which is consistent with slightly weaker entrainment rates.

b. Open questions

Although the simulations capture many aspects of the observational record, some questions as to their fidelity remain. These are touched on below as they are worth bearing in mind, both as a guide to future work and when interpreting the remainder of this study.

The quantitative relationship between drizzle rates and cloud droplet concentrations in our simulations is questionable. The original GCSS prescription specified cloud droplet concentrations of 55 cm^{-3}, more than twice as high as what we prescribe. Initial simulations with these higher concentrations produced too little precipitation. Simulations based on the model developed by Khairoutdinov and Kogan (2000) produced even less drizzle for a given droplet concentration. This tendency for large-eddy simulation to underrepresent precipitation is not limited to the current work nor to bulk models. Xue et al. (2008) require very low droplet concentrations to initiate precipitation in bin-resolved microphysical representations of trade wind cumulus. Similarly, Stevens et al. (1998) required both artificially low concentrations of cloud droplets and an artificially moist free troposphere.

Another physical issue that arises is the suggestion that the vertical stratification in thermodynamic quantities is too large in the DS and the vertical circulation is too weak. The DYCOMS-II measurements were not optimal for comparing the vertical structure in regions of precipitation with the vertical structure in nonprecipitating stratocumulus. However, the information they do provide suggests that the simulations might have too little variance in the vertical velocity; that is, the drizzle is overstabilizing the flow in the simulations and the simulated boundary layer might be less well mixed than what was observed. Measurements that can better constrain these aspects of the simulations would be useful.

Finally a numerical note: The use of monotone numerical schemes is required for an adequate representation of cloud-top processes (Stevens et al. 1996), but in our experience they come at the cost of a too dissipative representation of small scales, resulting in relatively poor (overly dissipative) representation of the inertial range in scalar variance, even if this aspect of the velocity variance is well represented; that is, this effect does not contributing to the impression that the simulations have too little vertical velocity variance. Being able to represent both the cloud-top processes and the range of small-scale variability within the boundary layer remains a challenging numerical issue, which may have physical implications.

4. Pools of elevated equivalent potential temperature

VanZanten et al. (2005) noted that pools of elevated θ_e were associated with precipitating regions in their

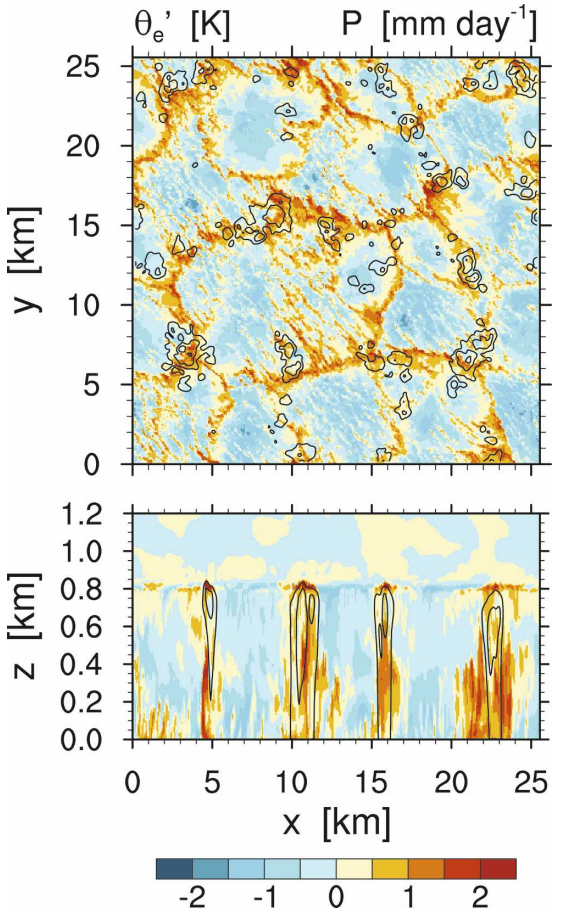

FIG. 10. (top) Instantaneous fields of perturbation of θ_e from horizontal mean and smoothed precipitation at 90-m height level at the end of the sixth hour of DS simulation. (bottom) Vertical cross section at $y = 45$ m of the instantaneous θ_e perturbations from the horizontal averages and horizontally smoothed precipitation at the end of the sixth hour of the DS simulation. Precipitation contours have values of 2, 10, and 30 mm day^{-1}.

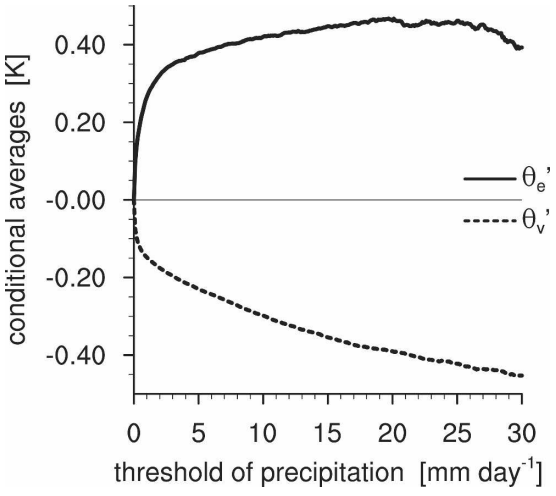

FIG. 11. Conditional average of θ'_e and θ'_v based on the strength of precipitation at 90-m height level at the end of the sixth hour of DS simulation.

analysis of in situ observations of precipitating stratocumulus. Similar features are prominent in the DS. For instance, as illustrated by Fig. 10, areas of precipitation tend to be collocated with the areas of elevated θ_e, most strikingly in the subcloud layer where they are observed, but also through the depth of the PBL. Figure 11 attempts to quantify this association by plotting θ_e averaged over those points whose precipitation rate exceeds some threshold versus this threshold. Averaged over all precipitating regions, θ_e is up to 0.1 K warmer than the domain average with the degree of the mean θ_e anomaly increasing with precipitation amount. Averaging just over regions of showers (i.e., where precipitation rates exceed 1 cm day^{-1}), θ_e anomalies approach 0.5 K. However, because to a first approximation θ_e is conserved under precipitation, it seems natural to ask (as did vanZanten et al. 2005) what leads to the elevated regions of θ_e.

This question is even more puzzling as the virtual potential temperature, θ_v, a perturbation of which is a proxy of buoyancy, behaves as expected: in the presence of precipitation it has lower values because the evaporation of drizzle acts as a sink of buoyancy. As illustrated by Fig. 11, composites for θ_v indeed exhibit negative anomalies (cold pools) in the precipitating areas. Similar behavior was also observed by Paluch and Lenschow (1991), who in the presence of drizzle estimated negative correlation between temperature and moisture on the mesoscales.

The simulations help us address the question of the source of the elevated θ_e in the precipitating regions. Because precipitation tends to stabilize the flow and hence reduce the vertical mixing and subsequent homogenization of the STBL, there is a general tendency of the precipitating simulations to have larger vertical gradients in thermodynamic quantities (particularly for moisture: e.g., Fig. 6). In Fig. 5, this tendency is manifest in the concentration of large values of θ_e near the surface. This suggests that regions of anomalously high θ_e might be a tracer of mesoscale circulations that channel near-surface air, which is rich in θ_e, into the interior of the flow. Figure 5 supports this line of thought as the precipitating regions, which collocate with regions of elevated θ_e, are also the regions where updrafts concentrate, presumably in the form of cumulus clouds.

a. Conditional sampling

To explore these ideas further, we form conditional averages of θ_e and w over the strongest θ_e events in the

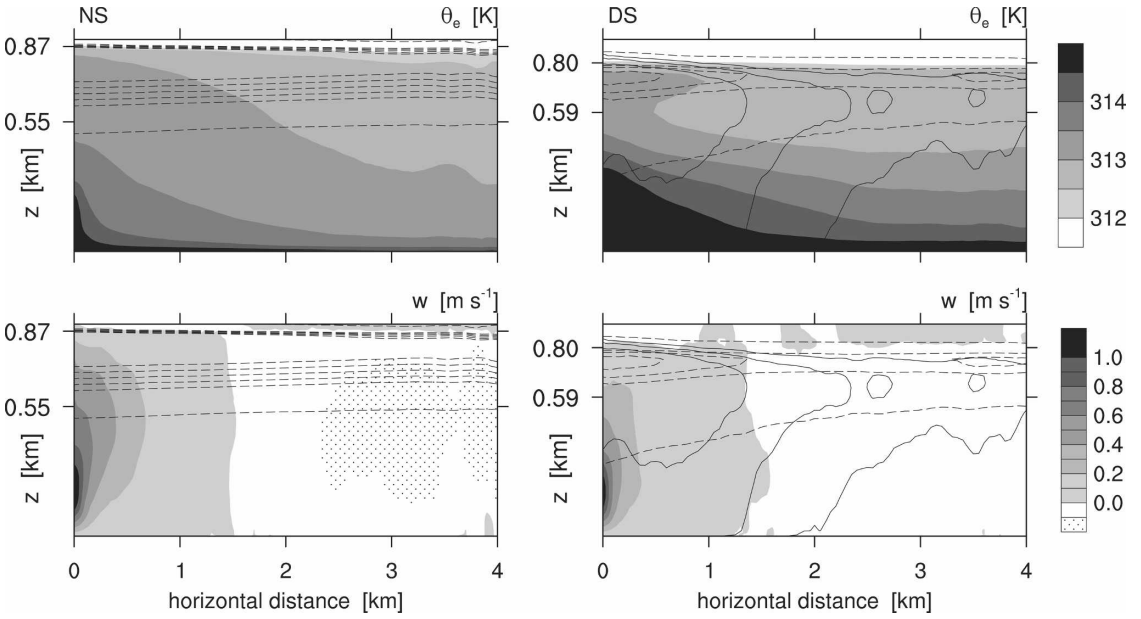

FIG. 12. Conditional composites of θ_e, w, r_l, and precipitation over the 40 strongest θ_e cells averaged over three independent times. Dashed contours represent r_l and have values of 0.01, 0.2, 0.25, 0.3, 0.35, and 0.4 g kg^{-1}. Solid contours represent precipitation intensities of 0.5, 1, 2, 5, and 10 W m^{-2}. Values on y axes as in Fig. 6. Left column is NS and right column is DS.

NS and the DS, which we refer to as θ_e cells. The conditional averaging follows the approach outlined by Schmidt and Schumann (1989), with details provided in appendix B. The flow, conditionally averaged in this way (Fig. 12), provides support for these ideas. Not only does it show anomalous stratification of θ_e in the DS simulations, but also an association of θ_e cells with both precipitation and updrafts. The latter are key in transporting air rich in θ_e away from the surface.

For the precipitating simulations, these questions are also usefully explored by examining the structure of the flow conditionally averaged on drizzle (Fig. 13), or what

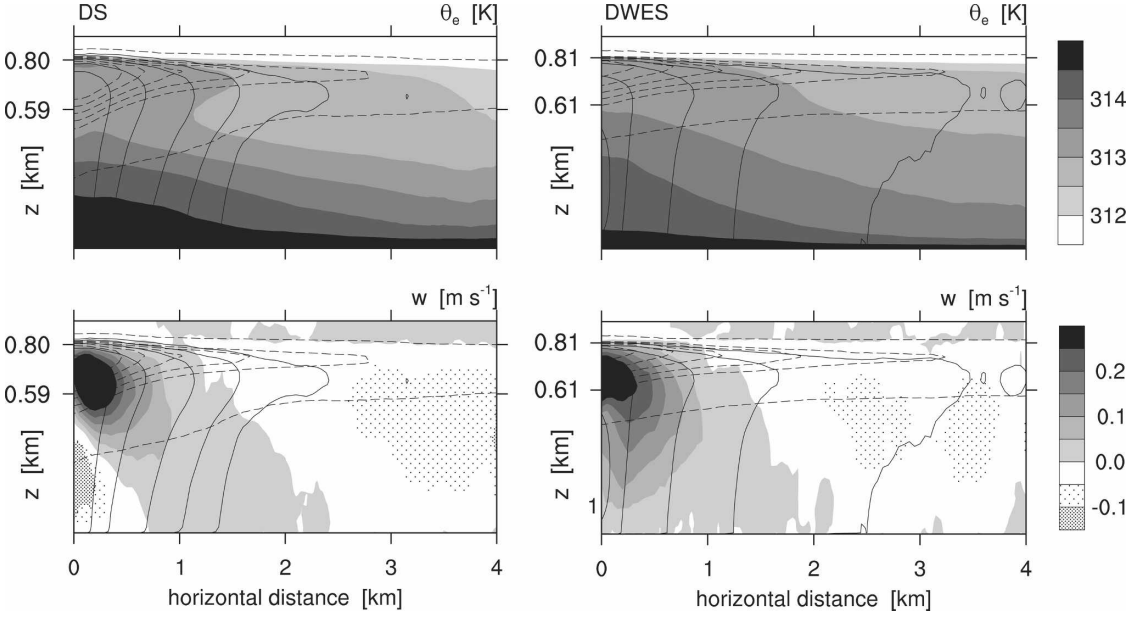

FIG. 13. As in Fig. 12 but for the drizzling cells. Left column is DS and right column is DWES.

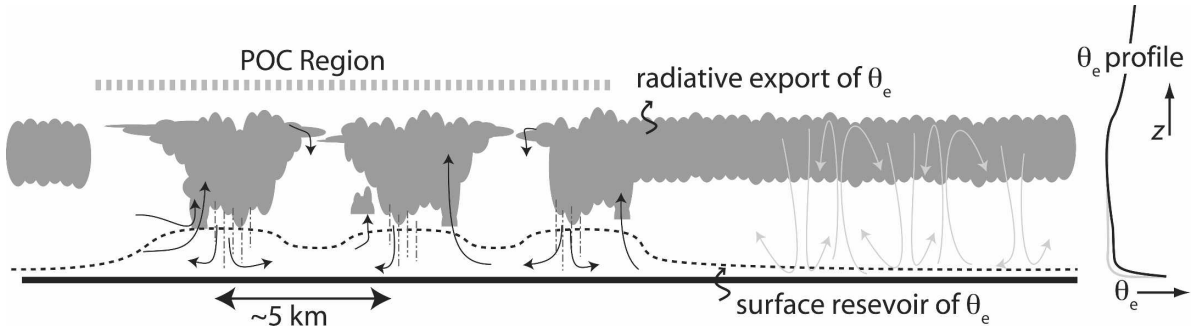

FIG. 14. Generalization of cartoon from vanZanten et al. (2005) conceptualizing the circulation and its effects on cloud and θ_e. Here the behavior in nonprecipitating stratocumulus (including mean profiles of θ_e) is shown in gray alongside precipitating regions (darkened).

we call drizzling cells. Conditionally sampling in this way confirms the previous association of drizzling areas in the DS with the pools of elevated θ_e. It also reveals subtle differences between θ_e and drizzling cells. Peak values of θ_e tend to be just off the center of the drizzling cell, which suggests that the precipitation maximizes on the edge of θ_e cells. This agrees well with the tilted position of the updrafts in the drizzling cells of the DS, also evident in Fig. 13: one interpretation of this is that new cumulus cells form on the outflow boundaries of evaporating precipitation (i.e., the θ_e-rich cold pools) and that they are accompanied by midlevel inflow (e.g., Comstock et al. 2007).

Figure 13 also helps illustrate the effect of evaporation of drizzle on the flow. Whereas evaporation leads to the development of a pronounced downdraft at the base of the drizzling cell (the evaporating rain shaft), such a feature is absent in the DWES. As a result, the updraft, and the associated region of precipitation, tends to be more spatially diffuse in the DWES, perhaps reflecting the lack of outflow boundaries in the absence of evaporation of precipitation. The suggestion that the coupling between the cloud and subcloud layer is more spatially compact in the DS simulations is consistent with the emergence of a mushroom- (or anvil-) like character of the cloud layer θ_e field in the DS drizzling cells and the lack of such a feature in the drizzling cells of the DWES. It is also consistent with simulations of trade wind cumulus (Xue et al. 2008) and some previous observational analyses of shallow convection (Jensen et al. 2000), which show that precipitation helps control the organization of new cloud formation, largely confining it to boundaries marking the edge of outflow from the precipitating downdrafts.

b. Conceptual diagram

In Fig. 14, we summarize some of the insights of the previous analysis in the form of a conceptual diagram, or a cartoon. In particular, we illustrate the tendency of strong drizzle (in our simulations about 1 mm day^{-1}) to drive a transition from a well-mixed stratocumulus-topped boundary layer driven by radiation and downdrafts to a more cumulus-coupled, or cumulus-under-stratocumulus-topped, layer. Our ability to quantify how different processes contribute to such a transition is the subject of an ongoing study. Here, the drizzling regime is described as well as how it differs from the nondrizzling one.

The cartoon depicts that, in agreement with the observations (vanZanten et al. 2005; Comstock et al. 2005), precipitation tends to be located in patches where the cloud base is lower and motions are carried by more cumulus-like circulations. In these regions, θ_e is higher and updrafts are more vigorous. Away from these regions, the circulations are weaker and may even be cloud free in places. There is also less evidence of downdrafts that mix through the depth of the layer, such as are characteristic of the nonprecipitating STBL.

The changes in the turbulent structure of the flow that accompany drizzle allow for greater differentiation in conserved tracers. Specifically, reduced mixing throughout the boundary layer allows θ_e to accumulate near the source of θ_e at the surface. This vertical differentiation can lead to horizontal differentiation in the presence of coherent updrafts. For instance, the updrafts in the drizzling regime draw on a richer reservoir of θ_e as compared to the updrafts in the nondrizzling one. The tendency of updrafts to be more localized (cumulus like) in the presence of precipitation amplifies the contrast in θ_e between updraft regions and the environment above the surface layer. Finally, because updrafts tend to be concentrated in or at the boundary of the precipitation shafts, regions of elevated θ_e appear collocated (or near so) with regions of precipitation. This may provide an explanation of why the pools of elevated θ_e became detectable by aircraft measure-

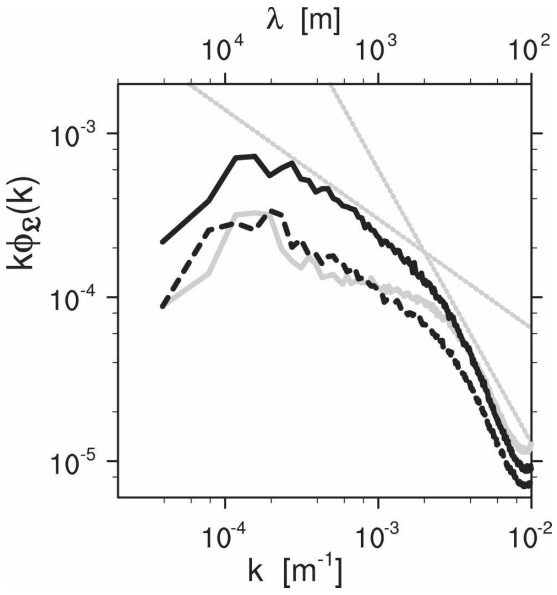

FIG. 15. Power spectra of the liquid water path in the simulations. Choice of lines follows Fig. 2. Dotted lines show a −2/3 and −5/3 spectra, respectively.

ments in the drizzling parts of RF02 of DYCOMS-II (vanZanten et al. 2005).

To the extent that our simulations are correct, the highest values of θ_e will not be found directly in the precipitation shafts—rather, on the sides where air is being most actively drawn out of the surface layer. It is still unclear if these θ_e-rich updrafts are the source of new cells or if they simply reflect a circulation that supports already existing drizzling cells with the necessary θ_e. Both of these might explain the long-lasting steady precipitation over the domain as a whole, and are a subject of our further investigation.

5. Discussion

a. Scales of variance

To what extent does precipitation engender, or promote, the development of meso-γ-scale variance in the simulations? From Fig. 1 it is clear that variance develops at larger scales in all the simulations, irrespective of the development of drizzle. This tendency toward the development of larger scales in all quantities other than w is evident in the steady increase in boundary layer integrated turbulence kinetic energy (lower panel of Fig. 9). The increase in TKE is due to increases in the horizontal velocity variances, and spectra show these to be increasing with time at the largest scales. Visualizations of the evolution of albedo show a similar trend and are reminiscent of the results of de Roode et al. (2004), which suggests that the underlying conditions for the emergence of large scales is the same as that reported by Jonker et al. (1999) and not dependent on the development of precipitation. Such a result would also be consistent with the observations of Wood and Hartmann (2006) who find no systematic difference between the aspect ratios of open and closed cells.

TABLE 1. Domain-averaged albedo, liquid water path, and cloud fraction for both small and large domain simulations over the last two hours of the simulation.

Simulation size (km)	NS		DS	
	6.4	25.6	6.4	25.6
A (%)	69.9	73.0	28.1	34.5
$\mathcal{L}$ (g m^{-2})	103.9	122.1	38.3	50.4
C (%)	99.9	100.0	88.7	95.4

Precipitation does, however, seem to enhance the accumulation of large-scale variance in our simulations. This is evident in Fig. 15, which shows the power spectrum of liquid water path from the simulations. Although the variance at small scales is probably too damped, for reasons discussed above, these spectra show that all of the simulations develop significant variance at large scales but that this accumulation is most pronounced for the DS. This increase in variance at large scales is also evident in the spectra of θ_l and r_t, particularly near the top of the boundary layer, and may reflect a less active cascade of variance to small scales in association with a weaker boundary layer circulations, or simply the effect of precipitation which acts as a source of θ_l and r_t and may thereby amplify any preexisting tendency toward the development of larger scales.

How important is the emergence of larger-scale variance to the mean properties of the simulations? Here we rejoin the question raised in the introduction regarding the reliability of simulations of these phenomena on much smaller domains. To address this question statistics from both large and small domain simulations are presented in Table 1. Overall, the small domain simulations seem to be biased toward lower amounts of cloud, cloud liquid water, and smaller albedo. The effects are more pronounced in the presence of precipitation; hence the simulations on the small domain exaggerate the effects of precipitation. One interpretation is that the compensating subsidence associated with the emergence of more cumulus-like cells is confined to too small a scale. Another possibility is that the growth of variance at larger scales favors the development of cloud. Notwithstanding these limitations, the small domain simulations do capture the main features of the simulations at larger scales, and the biases that one can

attribute to underrepresenting the range of scales are probably no greater than those associated with uncertainties in the representation of microphysical processes.

b. Consummating the transition

The simulations show that precipitation can lead to a marked transition in the planform structure of the cloud and that this transition evinces elements of a more open-cell, or POC-like, structure. That said, even by forcing drizzle with rather dramatic reductions in droplet concentrations, it is fair to say that the open-cell regime that we see in satellite images of pockets of open cells are not fully realized by the simulations. Are we missing something? One possibility is that the microphysical representation, either by producing too large of precipitation particles or through our neglect of ventilation effects or other processes, leads to insufficient evaporation in the subcloud layer. Or, that our use of a more active microphysical scheme (i.e., Seifert and Beheng 2001, as compared to Khairoutdinov and Kogan 2000), and perhaps unrealistically low droplet concentrations still underestimates the drizzle rate. Locally, vanZanten et al. (2005) find evidence for more intense precipitation than we measure, and more active evaporation. Because their data only partially sampled the region of open cells, it proves difficult to make such comparisons more quantitative. Even so, as a preliminary exploration of these ideas, we conducted a series of simulations in which we enhanced the evaporative effects of precipitation, but these did not produce a more marked open-cellular structure.

Another possibility is that other processes play an important role, for instance, the diurnal cycle. During daytime hours the additional desiccation of the thin layer of clouds, due to solar-radiative effects compensating the longwave cooling, may provide an additional forcing that helps consummate the transition to an open-cellular structure. We do, indeed, find that, if the DS is extended for an additional three hours without any radiative forcing (as a first approximation to the cancellation of longwave cooling by shortwave heating), the transition to a more completely open-cell structure is unambiguous (Fig. 16). Similar transitions, however, do not occur in simulations of this type performed using the NS as initial conditions. Here note that the cloud field in Fig. 16 is relatively steady and that, apart from the changes in the cloud field and the emergence of even larger scales, the principal difference with the DS is that in the absence of longwave cooling the cloud layer warms substantially. One objection to this line of argument could be that pockets of open cells are also evident in the nighttime imagery

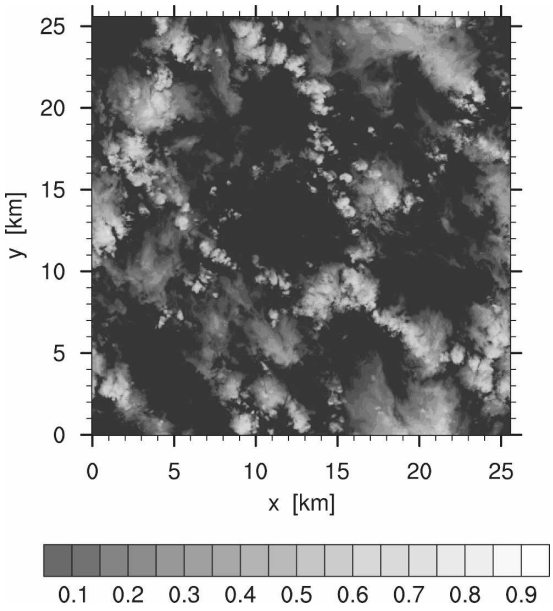

FIG. 16. Albedo, per Eq. (5), after three additional hours of simulation for the DS case but with the radiative forcing turned off.

(Petters et al. 2006), but perhaps this simply reflects the inability of the closed-cell pattern to reestablish itself after daytime desiccation. While these ideas are speculative, they can be tested, for instance, by looking to see whether the satellite record shows POCs more likely to form during the day or night or by simulations that more realistically and systematically treat the effects of the diurnal cycle.

6. Summary and conclusions

A simple, bulk, two-moment representation of microphysics is introduced into the UCLA LES to facilitate the study of precipitating stratocumulus. The use of such a simple scheme allows us to explore the interaction of microphysical, turbulent cloud dynamical and radiative processes over large spatial scales using fine spatial discretization.

Simulations of precipitating stratocumulus in large domains (25.6 km by 25.6 km) are shown to realistically represent many aspects of observed precipitating stratocumulus. These include the tendency of the layer to transition to more cumulus-coupled circulations, with locally elevated cloud tops and patches of anomalous subcloud equivalent potential temperature, θ_e, in the vicinity of precipitating clouds.

The simulations also capture the observed tendency for precipitation to be associated with the emergence of a more marked mesoscale circulation and a general reduction in cloudiness. Comparisons between precipitat-

ing and nonprecipitating simulations show a reduction in cloud albedo from near 75% in the absence of precipitation to values less than 35% in the presence of domain-averaged precipitation rates of around 1 mm day^{-1}. Most of this albedo reduction can be attributed to changes in the character of the circulation, as the reduction due to the Twomey effect can only account for about a third of the simulated albedo change. Although domain-averaged liquid water paths are reduced by half in the presence of drizzle, our simulations are able to maintain a nearly stationary evolution of the cloud in the presence of significant precipitation, in part because the stabilizing effect of precipitation reduces cloud-top entrainment, and hence entrainment drying. The stabilizing effect of precipitation is also evident in a reduction in vertical mixing, greater differentiation between the cloud and subcloud layer, and a marked increase in the variance of thermodynamic variables. The results provide support for inferences made from coarser resolution simulations with horizontal domains too small to represent mesoscale flow features. Analyses of the simulations suggest that the observed tendency of precipitation from shallow convection to collocate with patches of elevated values of subcloud equivalent potential temperature reflects the tendency of θ_e to accumulate near the surface in more stabilized precipitating flows, in concert with mesoscale circulations which concentrate precipitation within envelopes of upward motion.

A sensitivity study, in which the evaporation of precipitation-size drops is suppressed, shows that for this case the evaporation of precipitation is critical to the observed flow transition. While precipitation rates and liquid water paths are commensurate between precipitating simulations with and without evaporation, the transition of the flow to a cumulus-coupled state is only evident in the case when precipitation-size drops are allowed to evaporate below cloud base. Moreover, the subcloud circulations (cold pools and ensuing regions of lower cloud base) that ensue from such a process appear to play a vital role in shaping the structure of both the subcloud layer and regions of new convection.

Acknowledgments. Axel Seifert is kindly thanked for access to his original microphysical code, as well as his council regarding its use. Andrew Ackerman and Margreet vanZanten are thanked for their careful work in preparing such an interesting case for further study. Two anonymous reviewers and Robert Wood are thanked for their insightful and constructive suggestions on an earlier draft of this work. The first author would also like to thank Margreet vanZanten, Chris Holloway, Brian Medeiros, and Simona Bordoni for their unselfish support in all stages of this work. Computational resources were made available by NCAR and San Diego Supercomputer Center (SDSC). Financial support has been provided by NSF Grants ATM-0342625, 0336849, and 9985413.

APPENDIX A

Bulk Rain Formation

a. Microphysical processes

Microphysical processes currently present in the UCLA LES follow Seifert and Beheng (2001). In particular, intra- and interspecies interactions of cloud droplets and drizzle drops are modeled:[3]

1) AUTOCONVERSION

Drizzle formation occurs through intraspecies interaction of cloud droplets, that is, by collision and coalescence of cloud droplets. It augments both the mass and number of drizzle drops and is modeled as

$$C_{cc}(r_c, r_r; m^*, N_c) = \frac{k_c}{20m^*}\frac{(\upsilon_c + 2)(\upsilon_c + 4)}{(\upsilon_c + 1)^2} r_c^2 m_c^2 \times \left[1 + \frac{\phi_{\text{au}}}{(1 + \tau)^2}\right]\rho_0 . \quad (6)$$

Here, $m^* = 6.5 \times 10^{-11}$ kg is a separation mass between cloud droplets and drizzle drops that we chose to agree with the observations (vanZanten et al. 2005), while $m_c = r_c/N_c$ is the mean mass of cloud droplets. This value of m^* differs from the Seifert and Beheng (2001) and, together with the decrease of the n_c that we introduced, essentially has an impact of an increase of autoconversion rates, perhaps not incommensurately with what one might get as a result of turbulence effects (A. Seifert 2007, personal communication). Furthermore, $k_c = 9.44 \times 10^9$ m^3 kg^{-2} s^{-1} is a cloud-droplet-related coefficient in Long kernel, $\nu_c = 0$ corresponds to the Gamma distributed cloud droplets,

$$\tau = 1 - \frac{r_c}{r_c + r_r}, \quad \Phi_{\text{au}} = k_1 \tau^{k_2}(1 - \tau^{k_2})^3,$$

where $k_1 = 600$ and $k_2 = 0.68$, and ρ_0 is air density at the surface.

[3] UCLA LES is defined in terms of mixing ratios, while the work of Seifert and Beheng (2001, 2006) is based on the concentrations. To derive equations from Seifert and Beheng (2001, 2006), one needs to multiply the equations here with the air density ρ and follow with transformation of all the relevant terms.

2) ACCRETION

Growth of drizzle drops through interspecies interaction of drizzle drops and cloud droplets, that is, by collection of cloud droplets, increases the mean mass of drizzle and is modeled following

$$C_{cr}(r_c, r_r) = k_r r_c r_r \Phi_{\text{ac}} \sqrt{\rho_0 \rho}. \tag{7}$$

Here $k_r = 5.78\ \text{m}^3\ \text{kg}^{-1}\ \text{s}^{-1}$ is a drizzle-drop-related coefficient in Long kernel,

$$\Phi_{\text{ac}} = \left(\frac{\tau}{\tau + k_1}\right)^4,$$

with $k_1 = 5 \times 10^{-4}$ and ρ is air density.

3) SELF-COLLECTION

Growth of drizzle drops through intraspecies interaction of drizzle drops, that is, by collection of smaller drizzle drops by the larger ones, reduces the number of drizzle drops and is modeled as

$$C_{rr}(r_r, n_r) = -k_r n_r r_r \sqrt{\rho_0 \rho}. \tag{8}$$

b. Sedimentation

Sedimentation of drizzle drops in the UCLA LES is in accordance with what Seifert and Beheng (2001) used in their study (A. Seifert and K. D. Beheng 2005, personal communication). In particular, mass- and number-weighted mean fall velocities are modeled following

$$\upsilon_r(r_r, n_r) = 4a[1 - (1 + bD_m)^{-5}]D_m, \tag{9}$$

$$\upsilon_n(r_r, n_r) = a[1 - (1 + bD_m)^{-2}]D_m. \tag{10}$$

Here $a = 4 \times 10^3\ \text{m s}^{-1}$, $b = 12 \times 10^3\ \text{m}^{-1}$ and

$$D_m = [6r_r/(\pi \rho_l n_r)]^{1/3}$$

is the mean (mass) drizzle drop diameter. The sedimentation fluxes are then calculated using the upwind Eulerian scheme for both mass and number mixing ratios. However, only the sedimentation flux of mass mixing ratio of drizzle affects the evolution of the thermodynamic properties of the air.

Cloud droplet sedimentation flux in the UCLA LES is based on the mass-weighted mean fall velocities and is modeled as

$$F_c(r_c, N_c) = c[3/(4\pi \rho_l N_c)]^{2/3} \rho r_c^{5/3} \exp(5 \ln^2 \sigma_g), \tag{11}$$

where $c = 1.19 \times 10^8\ \text{m}^{-1}\ \text{s}^{-1}$ (Rogers and Yau 1989), σ_g is a geometric standard deviation, and ρ_l is the liquid water density.

c. Evaporation

Evaporation of drizzle drops in these simulations is modeled following Seifert and Beheng (2006) but neglecting the ventilation effect:

$$E(r_r, r_v, r_s, n_r) = 2\pi G S n_r D_m. \tag{12}$$

Here

$$G = \left[(\rho r_s D_v)^{-1} + \frac{L}{K_T T}\left(\frac{L}{R_v T} - 1\right)\right]^{-1},$$

with $K_T = 2.5 \times 10^{-2}\ \text{J s}^{-1}\ \text{K}^{-1}\ \text{m}^{-1}$ being heat conductivity, $D_v = 3 \times 10^{-5}\ \text{m}^2\ \text{s}^{-1}$ the diffusivity of water vapor, $R_v = 461\ \text{J kg}^{-1}\ \text{K}^{-1}$ the water vapor gas constant, and $S = r_v/r_s - 1$ the supersaturation. Drizzle drops are not allowed to grow through condensation, but instead condensation produces new, or increases mass of existing cloud droplets.

APPENDIX B

Conditional Sampling

Conditional composites in the θ_e and drizzling cells analyzed in section 4 are formulated following Schmidt and Schumann (1989), who define the conditional composites of the updraft cells to analyze the coherent features in the convective boundary layer. Here we present the steps taken in the construction of the cells. First, we locate the centers of the cells by identifying the local maxima of precipitation and θ_e at a given height level that are stronger than prescribed threshold values, which are referred to as events. Then, we isolate the strongest events by excluding the nearby weaker ones. To keep statistics comparable between the different simulations and the two types of cells, we choose only the 40 strongest maxima at the three selected independent times toward the end of simulations (5, 5.5, and 6 h). For precipitation we choose a threshold of 2 mm day^{-1} and for θ_e, 316 K. Both cells are defined based on the fields at 200-m height, and the exclusion distance we present here is 1600 m, which corresponds to about two boundary layer heights in the DS. After isolating the events, we define the areas encompassed by each cell as a cylinder with given radius and height throughout the whole domain such that there is no overlaying between the surrounding cells. We do so by mapping each point in the domain to its closest cell center and excluding all points that are more than 5 km away from the closest cell center. The conditional composites of w, θ_e, precipitation, and r_l presented in section 4 are finally constructed by first binning the fields by the horizontal distance from the centers of the cells and then averaging the values in each bin.

REFERENCES

Ackerman, A. S., M. P. Kirkpatrick, D. E. Stevens, and O. B. Toon, 2004: The impact of humidity above stratiform clouds on indirect aerosol climate forcing. *Nature,* **432,** 1014–1017.

Agee, E. M., 1984: Observations from space and thermal convection: A historical perspective. *Bull. Amer. Meteor. Soc.,* **65,** 938–949.

Albrecht, B. A., 1989: Aerosols, cloud microphysics, and fractional cloudiness. *Science,* **245,** 1227–1230.

Bretherton, C. S., and Coauthors, 2004: The EPIC 2001 stratocumulus study. *Bull. Amer. Meteor. Soc.,* **85,** 967–977.

Brost, R. A., D. H. Lenschow, and J. C. Wyngaard, 1982a: Marine stratocumulus layers. Part I: Mean conditions. *J. Atmos. Sci.,* **39,** 800–817.

——, J. C. Wyngaard, and D. H. Lenschow, 1982b: Marine stratocumulus layers. Part II: Turbulence budgets. *J. Atmos. Sci.,* **39,** 818–836.

Comstock, K. K., C. S. Bretherton, and S. E. Yuter, 2005: Mesoscale variability and drizzle in southeast Pacific stratocumulus. *J. Atmos. Sci.,* **62,** 3792–3807.

——, S. E. Yuter, R. Wood, and C. S. Bretherton, 2007: The three-dimensional structure and kinematics of drizzling stratocumulus. *Mon. Wea. Rev.,* **135,** 3767–3784.

de Roode, S. R., P. G. Duynkerke, and H. J. J. Jonker, 2004: Large-eddy simulation: How large is large enough? *J. Atmos. Sci.,* **61,** 403–421.

Jensen, J. B., S. Lee, P. B. Krummel, J. Katzfey, and D. Gogoasa, 2000: Precipitation in marine cumulus and stratocumulus. Part I: Thermodynamic and dynamic observations of closed cell circulations and cumulus bands. *Atmos. Res.,* **54,** 117–155.

Jonker, H. J. J., P. G. Duynkerke, and J. W. M. Cuijpers, 1999: Mesoscale fluctuations in scalars generated by boundary layer convection. *J. Atmos. Sci.,* **56,** 801–808.

Khairoutdinov, M., and Y. Kogan, 2000: A new cloud physics parameterization in a large-eddy simulation model of marine stratocumulus. *Mon. Wea. Rev.,* **128,** 229–243.

Nicholls, S., 1984: The dynamics of stratocumulus: Aircraft observations and comparisons with a mixed layer model. *Quart. J. Roy. Meteor. Soc.,* **110,** 783–820.

Orlanski, I., 1975: A rational subdivision of scales for atmospheric processes. *Bull. Amer. Meteor. Soc.,* **56,** 527–530.

Paluch, I. R., and D. H. Lenschow, 1991: Stratiform cloud formation in the marine boundary layer. *J. Atmos. Sci.,* **48,** 2141–2158.

Petters, M. D., J. R. Snider, B. Stevens, G. Vali, I. Faloona, and L. M. Russell, 2006: Accumulation mode aerosol, pockets of open cells, and particle nucleation in the remote subtropical Pacific marine boundary layer. *J. Geophys. Res.,* **111,** D02206, doi:10.1029/2004JD005694.

Pincus, R., and M. B. Baker, 1994: Effect of precipitation on the albedo susceptibility of clouds in the marine boundary layer. *Nature,* **372,** 250–252.

Rogers, R. R., and M. K. Yau, 1989: *A Short Course in Cloud Physics.* 3rd ed. Butterworth-Heinemann, 290 pp.

Schmidt, H., and U. Schumann, 1989: Coherent structure of the convective boundary layer derived from large-eddy simulations. *J. Fluid Mech.,* **200,** 511–562.

Seifert, A., and K. D. Beheng, 2001: A double-moment parameterization for simulating autoconversion, accretion and self-collection. *Atmos. Res.,* **59–60,** 265–281.

——, and ——, 2006: A two-moment cloud microphysics parameterization for mixed-phase clouds. Part 1: Model description. *Meteor. Atmos. Phys.,* **92,** 45–66.

Sharon, T. M., B. A. Albrecht, H. H. Jonsson, P. Minnis, M. M. Khaiyer, T. M. van Reken, J. Seinfeld, and R. Flagan, 2006: Aerosol and cloud microphysical characteristics of rifts and gradients in maritime stratocumulus clouds. *J. Atmos. Sci.,* **63,** 983–997.

Siebesma, A. P., and Coauthors, 2003: A large eddy simulation intercomparison study of shallow cumulus convection. *J. Atmos. Sci.,* **60,** 1201–1219.

Stevens, B., 2000: Cloud transition and decoupling in shear-free stratocumulus-topped boundary layers. *Geophys. Res. Lett.,* **27,** 2557–2560.

——, G. Feingold, W. R. Cotton, and R. L. Walko, 1996: Elements of the microphysical structure of numerically simulated nonprecipitating stratocumulus. *J. Atmos. Sci.,* **53,** 980–1006.

——, W. R. Cotton, G. Feingold, and C.-H. Moeng, 1998: Large-eddy simulations of strongly precipitating, shallow, stratocumulus-topped boundary layers. *J. Atmos. Sci.,* **55,** 3616–3638.

——, and Coauthors, 2003: Dynamics and chemistry of marine stratocumulus—DYCOMS-II. *Bull. Amer. Meteor. Soc.,* **84,** 579–593.

——, and Coauthors, 2005a: Evaluation of large-eddy simulations via observations of nocturnal marine stratocumulus. *Mon. Wea. Rev.,* **133,** 1443–1462.

——, G. Vali, K. K. Comstock, R. Wood, M. C. vanZanten, P. H. Austin, C. S. Bretherton, and D. H. Lenschow, 2005b: Pockets of open cells and drizzle in marine stratocumulus. *Bull. Amer. Meteor. Soc.,* **86,** 51–57.

Vali, G., R. D. Kelly, J. French, S. Haimov, D. Leon, R. E. McIntosh, and A. Pazmany, 1998: Finescale structure and microphysics of coastal stratus. *J. Atmos. Sci.,* **55,** 3540–3564.

vanZanten, M. C., and B. Stevens, 2005: Observations of the structure of heavily precipitating marine stratocumulus. *J. Atmos. Sci.,* **62,** 4327–4342.

——, ——, G. Vali, and D. H. Lenschow, 2005: Observations of drizzle in nocturnal marine stratocumulus. *J. Atmos. Sci.,* **62,** 88–106.

Wood, R., and D. L. Hartmann, 2006: Spatial variability of liquid water path in marine low cloud: The importance of mesoscale cellular convection. *J. Climate,* **19,** 1748–1764.

Xue, H., G. Feingold, and B. Stevens, 2008: Aerosol effects on clouds, precipitation, and the organization of shallow cumulus convection. *J. Atmos. Sci.,* **65,** 392–406.

Zhang, Y., B. Stevens, and M. Ghil, 2005: On the diurnal cycle and susceptibility to aerosol concentration in a stratocumulus-topped mixed layer. *Quart. J. Roy. Meteor. Soc.,* **131,** 1567–1583.